JCTC Journal of Chemical Theory and Computation

Article

pubs.acs.org/JCTC

Efficient Calculation of Free Energy Differences Associated with Isotopic Substitution Using Path-Integral Molecular Dynamics

Ondrej Marsalek,[†] Pei-Yang Chen,[†] Romain Dupuis,[‡] Magali Benoit,[§] Merlin Méheut,[‡] Zlatko Bačić,[†,#] and Mark E. Tuckerman*[,⊥,∥,#]

[†]Department of Chemistry, New York University, New York, New York 10003, United States

[‡]Géosciences Environnement Toulouse, OMP—Université Paul Sabatier, 14 avenue Edouard Belin, 31400 Toulouse, France

[§]CEMES—CNRS—UPR 8011, 29 rue Jeanne Marvig, 31055 Toulouse, France

[⊥]Department of Chemistry and Courant Institute of Mathematical Sciences, New York University, New York, New York 10003, United States

[∥]Institute for Pure and Applied Mathematics, 460 Portola Plaza, Los Angeles, California 90095, United States

[#]NYU-ECNU Center for Computational Chemistry at NYU Shanghai, Shanghai 200062, China

Supporting Information

ABSTRACT: The problem of computing free energy differences due to isotopic substitution in chemical systems is discussed. The shift in the equilibrium properties of a system upon isotopic substitution is a purely quantum mechanical effect that can be quantified using the Feynman path integral approach. In this paper, we explore two developments that lead to a highly efficient path integral scheme. First, we employ a mass switching function inspired by the work of Ceriotti and Markland [*J. Chem. Phys.* **2013**, *138*, 014112] that is based on the inverse square root of the mass and which leads to a perfectly constant free energy derivative with respect to the switching parameter in the harmonic limit. We show that even for anharmonic systems, this scheme allows a single-point thermodynamic integration approach to be used in the construction of free energy differences. In order to improve the efficiency of the calculations even further, however, we derive a set of free energy derivative estimators based on the fourth-order scheme of Takahashi and Imada [*J. Phys. Soc. Jpn.* **1984**, *53*, 3765]. The Takahashi—Imada procedure generates a primitive fourth-order estimator that allows the number of imaginary time slices in the path-integral approach to be reduced substantially. However, as with all primitive estimators, its convergence is plagued by numerical noise. In order to alleviate this problem, we derive a fourth-order virial estimator based on a transferring of the difference between second- and fourth-order primitive estimators, which remains relatively constant as a function of the number of configuration samples, to the second-order virial estimator. We show that this new estimator converges as smoothly as the second-order virial estimator but requires significantly fewer imaginary time points.

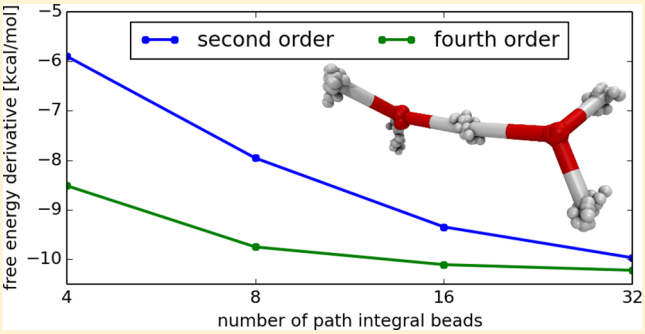

1. INTRODUCTION

Nuclear quantum effects influence substantially the physical properties of many systems, especially those containing lighter nuclei. The terms zero point energy and quantum tunnelling are often mentioned in this context, although they are just specific manifestations of a more complex phenomenon. While nuclear quantum effects increase with decreasing temperature, they can be substantial even at ambient conditions for many systems. One of the ways they manifest is the dependence of physical properties at equilibrium on the masses of nuclei, which vanishes in the classical limit. Therefore, isotopic substitution provides an experimental framework in which nuclear quantum effects can be directly probed. As an example, the freezing point of heavy water is almost 4 K above the freezing point of water. Assuming the Born—Oppenheimer approximation, the potential energy hypersurface generated by the electronic part of the system is entirely independent of the masses of the nuclei and thus all nuclear quantum effects are determined by the behavior of the nuclear part of the system on this hypersurface.

An important quantity associated with isotopic change is the free energy difference corresponding to the exchange. While this difference is trivial for a free particle, in all other situations it depends on the composition and thermodynamic state of the environment of an atom or atoms undergoing isotopic exchange. This results in different isotope ratios in different environments which are in chemical equilibrium. The equilibrium isotope fractionation factor is defined as the Boltzmann factor:

Received: October 20, 2013
Published: February 5, 2014

 © 2014 American Chemical Society

$$\alpha_{1-2} = \exp(-\beta(\Delta A_1 - \Delta A_2)) \quad (1)$$

where ΔA_1 and ΔA_2 are free energy differences upon isotope substitution in the two media, and $\beta = 1/k_B T$. This quantity relates to the isotopic ratios R (e.g., R = D/H, deuterium/hydrogen ratio) in the two media through:

$$\alpha_{1-2} = \frac{R_1}{R_2} \quad (2)$$

For example, the different isotopic ratios D/H in the liquid and vapor phases of water can be used in climate analysis.[1] On the other hand, the lithium isotope system (^{6}Li/^{7}Li) has been extensively used to understand the chemical processes that occur during the subduction of tectonic plates.[2,3] It is also considered as a very promising tool to constrain weathering processes and the CO_2 global cycle.[4] In these situations, the fractionation of interest occurs between Li in water and Li in minerals. Computation of the free energy of isotopic substitution of solvated Li^+ is, therefore, of considerable interest.

The methods of thermodynamic integration[5] or free energy perturbation[6] can be used to calculate these free energy differences from molecular dynamics or, as suggested by Zimmermann and Vaníček,[7] Monte Carlo simulations. Ceriotti and Markland[8] employed a reweighting of the kinetic energy and free energy perturbation to calculate the isotope exchange free energy difference from a single simulation of one of the isotopes. In this paper, we will focus on the use of thermodynamic integration to treat this problem. Depending on the specific application, either a single atom or many atoms contribute to the free energy change. In the case of a hydrated lithium cation in the infinite dilution limit, for example, the mass of a single atom is changed while the rest of the system serves as its environment. The case of a single H_2O changing to an HOD in liquid water is an example in which a single atom changes mass; however, this change can occur in any of the equivalent water molecules in the system. Fully deuterating a liquid H_2O sample would clearly involve the simultaneous mass change of many atoms in the system, all of which would contribute to the free energy difference. Finally, quantum sieving through, for example, a modified 2D graphene sheet[9−11] is a technique by which isotopes of small gas molecules such as H_2 or He can be separated, suggesting very different free energy changes for the passage of one isotope versus the other through the sieve.

Imaginary time path integrals provide a robust and systematic way to include nuclear quantum effects in molecular and condensed-phase simulations.[12] The method is based on the formulation of the quantum canonical density matrix and partition function as a weighted sum over thermal paths. The partition function, in particular, requires that the paths be periodic in imaginary time with a period of $\beta\hbar$. When the paths are discretized for numerical implementation, they become isomorphic to ring polymers composed of a fixed number of points or "beads". Each bead is coupled to its nearest neighbors by a harmonic spring, the strength of which depends on $k_B T$. For many-particle systems treated as Boltzmann particles, each time slice through the imaginary time axis is a complete replica of the system. This formulation is exact in the limit of an infinite number of beads, but in practice, convergence of a given property of interest is checked, and a suitable finite number of beads is used. Potential energy surfaces for path integral calculations must approximate the true ground-state Born−Oppenheimer surface and should not, therefore, be parametrized to target specific physical properties obtained from experiment. Most experimental force fields are developed in this way and, therefore, will reproduce these properties in classical simulations. Thus, they implicitly contain the influence of nuclear quantum effects in their effective parameters. As an example, traditional water models are not suitable for use with path-integral simulations and must be adapted. Anharmonic bonded terms turn out to be important for the correct description of the balance between intermolecular and intramolecular nuclear quantum effects.[1] For these reasons, electronic structure methods represent a natural choice for combination with path integrals, as they aim to approximate the bare potential energy hypersurface for the nuclei. Because of this match of ab initio methods and path integrals,[39,40] it is important to develop methods that are efficient with such a combination, particularly given that path integral simulations are substantially more expensive than classical simulations for the same system. Sampling of the system of replicas can then be performed using either Monte Carlo or molecular dynamics. In this paper, we propose the use of efficient estimators for the kinetic energy combined with a thermodynamic integration scheme that requires only a few points and a small number of replicas to converge the calculation of the free energy differences associated with isotopic substitution.

In order to test the proposed methodology, we apply it to several systems with different properties. One-dimensional model systems (the harmonic oscillator and double well potentials) allow analysis of the methods under well-defined conditions and comparison to exact analytical or numerical results. Small molecular clusters allow the use of more accurate post-Hartree−Fock ab initio methods together with sufficient sampling to thoroughly test the methodology, which can then be directly used for simulations of larger cluster or condensed-phase systems, typically in combination with density functional theory. The results of these cluster calculations are also interesting in their own right and can serve as a benchmark for methods that are computationally less expensive but also less accurate. The HF dimer is a fundamental model of the hydrogen bond, and previous calculations of $(HF)_2$, $(DF)_2$, and HFDF[13] show that upon deuteration, stronger vibrational mode mixing occurs, which renders an unambiguous assignment of the low-lying states in vibrational spectra somewhat less clear. The water dimer is a basic model of the hydrogen bond and the substitution of hydrogen for deuterium is very common, especially in aqueous systems. Furthermore, introducing a proton defect into the system, by either adding or removing a proton while keeping the number of electrons constant, creates a delocalized proton in the system.[14] Quantum effects on this proton are different from those on protons in pure water systems, as the charge defect is not locked in a simple OH bond but rather shared by the two oxygens. We perform simulations of all these three variants of the water dimer, substituting all the hydrogen nuclei for deuterium nuclei in all cases. The lithium cation is an interesting target for *ab initio* path-integral molecular dynamics (AIPIMD) simulations for several reasons. A correct description of the hydration of this species is challenging for empirical force fields due to the high charge density of the ion, which results in substantial polarization of the solvent molecules as well as intermolecular charge transfer.[15] While this problem can be mitigated using either polarizable or charge transfer force fields or the electronic continuum correction, ab

initio methods represent an alternative that describes these effects more accurately and is more robust. From the perspective of quantum nuclear effects, lithium has a relatively light nucleus and is not covalently bound to any atoms. The effective potential created by its solvent shell can be expected to be more anharmonic than that of a proton in a water molecule, for example. Calculations of free energy differences upon isotope substitution and the resulting isotope fractionation ratios are interesting from the perspective of the above-mentioned applications, and it is, therefore, important to investigate the performance of the methodology for this type of system before attempting extensive condensed-phase simulations. To this end, we microhydrate the lithium cation with its first solvent shell of four water molecules[15,16] and perform an isotope substitution from ^{6}Li to ^{7}Li.

The rest of the paper is organized as follows. In the Theory section, we review the calculation of free energy differences upon isotope substitution by thermodynamic integration via path integrals. Existing path-integral estimators of the quantum kinetic energy, which are needed for these calculations, are introduced and their limitations are discussed. We introduce a new estimator that combines the advantages of fourth-order convergence and virial estimators. Finally, we introduce a mass switching function $m(\lambda)$ designed for accurate thermodynamic integration using only a few points. Next, we specify the computational details of our path-integral simulations. The Results section shows the data obtained using our methodology for the two model systems and four molecular systems. The performance of the methodology is discussed in relation to the properties of the different systems as well as in the context of other work on the topic. We conclude by summarizing the work and suggesting possible future directions.

2. THEORY

We consider an N-particle quantum system with a Hamiltonian $\hat{H} = \hat{T} + \hat{V}$ in which we wish to change the masses of $n \leq N$ of the particles. We parametrize the mass change from one isotope to another using a mass switching function $m_i(\lambda)$, $\lambda \in [0,1]$ that satisfies the boundary conditions $m_i(0) = m_{i,0}$, $m_i(1) = m_{i,1}$. While arbitrary, in principle, the choice of this function should be guided by the requirement of optimizing the efficiency of the calculation, as we discuss below. The Helmholtz free energy of a system, which is given by

$$A = -\beta^{-1} \ln Q = -\beta^{-1} \ln \mathrm{Tr}[e^{-\beta\hat{H}}] \tag{3}$$

where Q is the partition function, then becomes a function of λ through the dependence of the kinetic energy $\hat{T}$ on mass. The difference of free energies between the two states of interest can be calculated using thermodynamic integration as

$$\Delta A = A(1) - A(0) = \int_0^1 \frac{\mathrm{d}A}{\mathrm{d}\lambda}\,\mathrm{d}\lambda \tag{4}$$

The derivative of free energy with respect to λ is therefore the central quantity that needs to be calculated. It can be shown that it is given by the ensemble average of the kinetic energy operator $\hat{T}_i$ for particle i as

$$\frac{\mathrm{d}A}{\mathrm{d}\lambda} = -\sum_{i=1}^{N} \frac{1}{m_i(\lambda)} \frac{\mathrm{d}m_i}{\mathrm{d}\lambda} \langle \hat{T}_i \rangle \tag{5}$$

We derive this expression in the Appendix, together with the expression for the second derivative. Clearly, atoms whose mass does not change with λ do not contribute to the free energy change.

We formulate the calculation of the kinetic energy expectation in terms of a discretized imaginary-time path integral. Assuming that the particles obey Boltzmann statistics, the partition function can be written as an integral over N cyclic paths, each having P coordinates $\mathbf{r}_i^{(k)}$, where $i = 1, ..., N$ and $k = 1, ..., P$ indexes the imaginary time values $\tau_k = (k - \beta\hbar/P)$. These satisfy the path periodicity condition $\mathbf{r}_i^{(1)} = \mathbf{r}_i^{(P+1)}$. In terms of these, the partition function can be written as

$$\begin{aligned} Q &= \mathrm{Tr}[e^{-\beta\hat{H}}] \\ &= \int \left[\prod_{i=1}^{N} \left(\frac{m_i P}{2\pi\beta\hbar^2} \right)^{3P/2} \mathrm{d}\mathbf{r}_i^{(1)} \cdots \mathrm{d}\mathbf{r}_i^{(P)} \right] e^{-\beta V_{\mathrm{eff}}(\{\mathbf{r}\})} \end{aligned} \tag{6}$$

where $\{\mathbf{r}\}$ is the complete set of $3NP$ path coordinates and $V_{\mathrm{eff}}(\{\mathbf{r}\})$ is an effective potential. Equation 6 is derived by writing the Boltzmann operator as

$$e^{-\beta(\hat{T}+\hat{V})} = [e^{-\beta(\hat{T}+\hat{V})/P}]^P \tag{7}$$

and applying a Trotter expansion to the high-temperature Boltzmann operator $\exp[-\beta(\hat{T} + \hat{V})/P]$. For example, if a second-order Trotter expansion

$$e^{-\beta(\hat{T}+\hat{V})/P} = e^{-\beta\hat{V}/2P} e^{-\beta\hat{T}/P} e^{-\beta\hat{V}/2P} + O\left(\left(\frac{\beta}{P}\right)^3\right) \tag{8}$$

is used, then the second-order effective potential is given by

$$\begin{aligned} V_{\mathrm{eff}}^{(2)}(\{\mathbf{r}\}) = \frac{{\omega_P}^2}{2} \sum_{i=1}^{N} \sum_{k=1}^{P} m_i (\mathbf{r}_i^{(k)} - \mathbf{r}_i^{(k+1)})^2 \\ + \frac{1}{P} \sum_{k=1}^{P} V(\mathbf{r}^{(k)}) \end{aligned} \tag{9}$$

where $\omega_P = \sqrt{P/(\beta\hbar)}$ and $\mathbf{r}^{(k)}$ is the set of $3N$ coordinates for the kth imaginary time slice. The ensemble average of an operator $\hat{O}$ can be calculated from its estimator $O(\{\mathbf{r}\})$ as

$$\langle \hat{O} \rangle_{(2)} = \frac{\int \prod_{i=1}^{N} \prod_{k=1}^{P} \mathrm{d}\mathbf{r}_i^{(k)} O(\{\mathbf{r}\}) \exp(-\beta V_{\mathrm{eff}}^{(2)}(\{\mathbf{r}\}))}{\int \prod_{i=1}^{N} \prod_{k=1}^{P} \mathrm{d}\mathbf{r}_i^{(k)} \exp(-\beta V_{\mathrm{eff}}^{(2)}(\{\mathbf{r}\}))} \tag{10}$$

Specifically for the kinetic energy, one possible estimator is

$$T_i^{(\mathrm{prim})}(\{\mathbf{r}\}_i) = \frac{3P}{2\beta} - \sum_{k=1}^{P} \frac{1}{2} m_i {\omega_P}^2 (\mathbf{r}_i^{(k)} - \mathbf{r}_i^{(k+1)})^2 \tag{11}$$

which is known as the second-order "primitive" kinetic energy estimator. This estimator, however, has a variance that grows with the number of beads,[17] which makes convergence of the average increasingly slow as P increases. This problem can be circumvented by using the centroid virial estimator instead.[17,18] The virial theorem states that, at second order, $\langle T_i^{(\mathrm{prim})} \rangle = \langle T_i^{(\mathrm{vir})} \rangle$, where

$$T_i^{(\mathrm{vir})}(\{\mathbf{r}\}_i) = \frac{3}{2\beta} + \frac{1}{2P} \sum_{k=1}^{P} (\mathbf{r}_i^{(k)} - \mathbf{r}_{\mathrm{c},i}) \cdot \frac{\partial V}{\partial \mathbf{r}_i^{(k)}} \tag{12}$$

where $\mathbf{r}_{\mathrm{c},i}$ is the centroid position of particle i. This estimator has more favorable numerical properties, as its variance remains almost constant as P increases.[17]

dx.doi.org/10.1021/ct400911m | J. Chem. Theory Comput. 2014, 10, 1440−1453

Higher-order expansions of the Boltzmann operator increase the rate of convergence with respect to the number of path integral beads P[19,20] and were recently employed in Monte Carlo calculations of isotope effects by Vuchowiecki and Vaníček.[21] In the Takahashi–Imada scheme,[22,23] the *trace* of the Boltzmann operator is factorized according to

$$\mathrm{Tr}[e^{-\beta(\hat{T}+\hat{V})}] = \mathrm{Tr}[e^{-\beta\hat{T}/P}e^{-\beta\hat{C}/P}]^P + O\left(\left(\frac{\beta}{P}\right)^5\right) \tag{13}$$

where

$$\hat{C} = \hat{V} + \frac{\beta^2}{24P^2}[[\hat{V}, [\hat{T}, \hat{V}]] \tag{14}$$

Within this scheme, the effective potential becomes

$$V_{\mathrm{eff}}^{(4)}(\{\mathbf{r}\}) = V_{\mathrm{eff}}^{(2)}(\{\mathbf{r}\}) + V_{\mathrm{TI}}(\{\mathbf{r}\}) \tag{15}$$

with

$$V_{\mathrm{TI}}(\{\mathbf{r}\}) = \frac{1}{24P^2{\omega_P}^2}\sum_{i=1}^{N}\sum_{k=1}^{P}\frac{1}{m_i}\left(\frac{\partial V(\{\mathbf{r}\})}{\partial \mathbf{r}_i^{(k)}}\right)^2 \tag{16}$$

Because this potential contains the derivative of the physical potential V with respect to atomic positions, its use for path integral molecular dynamics, especially with ab initio path integrals, is impractical. Second derivatives of V with respect to positions are either expensive to calculate or entirely unavailable, depending on the method and implementation used. However, if V_{TI} is a small perturbation to the second-order effective potential, we can obtain averages at fourth-order by reweighting configurations from second-order dynamics using the weights

$$w_{\mathrm{TI}}(\{\mathbf{r}\}) = \frac{\exp(-\beta V_{\mathrm{TI}}(\{\mathbf{r}\}))}{\langle\exp(-\beta V_{\mathrm{TI}}(\{\mathbf{r}\}))\rangle_{(2)}} \tag{17}$$

as

$$\langle\hat{O}\rangle_{(4)}^{(\mathrm{prim})} = \langle O_{\mathrm{TI}}(\{r\})w_{\mathrm{TI}}(\{r\})\rangle_{(2)} \tag{18}$$

where $O_{\mathrm{TI}}(\{\mathbf{r}\})$ is an estimator derived using the fourth-order effective potential. Applying this scheme to the kinetic energy estimator, we obtain

$$T_{\mathrm{TI},i}^{(\mathrm{prim})}(\{\mathbf{r}\}_i) = \frac{3P}{2\beta} - \sum_{k=1}^{P}\frac{1}{2}m_i{\omega_P}^2(\mathbf{r}_i^{(k)} - \mathbf{r}_i^{(k+1)})^2 + V_{\mathrm{TI},i}(\{\mathbf{r}\}_i) \tag{19}$$

which is again a primitive estimator with the same numerical issues as its second-order counterpart. Here, $V_{\mathrm{TI},i}$ is the TI potential for particle i. Because the noise comes from the harmonic coupling term, we can expect the sampling error to be highly correlated in the second- and fourth-order estimators. In principle, the noise could be reduced at fourth-order in much the same was as it is at second-order by introducing a fourth-order virial estimator. However, as was shown in reference 20 such an estimator would require spatial derivatives of $V_{\mathrm{TI}}(\{\mathbf{r}\})$, i.e., second derivatives of the potential V, which, as noted above, need to be avoided. With this motivation, we propose a fourth-order virial estimator constructed by transferring the difference between the second- and fourth-order primitive estimators to the second-order virial estimator, which leads to the an expression of the form

$$T_{\mathrm{TI},i}^{(\mathrm{vir})}(\{\mathbf{r}\}) = T_i^{(\mathrm{vir})}(\{\mathbf{r}\}_i) + w_{\mathrm{TI}}(\{\mathbf{r}\})T_{\mathrm{TI},i}^{(\mathrm{prim})}(\{\mathbf{r}\}_i) - T_i^{(\mathrm{prim})}(\{\mathbf{r}\}_i) \tag{20}$$

which is meant to be averaged over configurations generated at second-order, leading to the average kinetic energy expression

$$\langle\hat{T}_i\rangle_{(4)}^{(\mathrm{vir})} = \langle T_i^{(\mathrm{vir})}(\{\mathbf{r}\}_i) + w_{\mathrm{TI}}(\{\mathbf{r}\})T_{\mathrm{TI},i}^{(\mathrm{prim})}(\{\mathbf{r}\}_i) - T_i^{(\mathrm{prim})}(\{\mathbf{r}\}_i)\rangle_{(2)} \tag{21}$$

Here, $\{\mathbf{r}\}_i$ denotes the full set of imaginary time slices for particle i. In practice, the result can be obtained by first calculating the ensemble averages of the quantum kinetic energy estimators on the right-hand individually and expressing the fourth-order virial estimator as

$$\langle\hat{T}_i\rangle_{(4)}^{(\mathrm{vir})} = \langle\hat{T}_i\rangle_{(2)}^{(\mathrm{vir})} + (\langle\hat{T}_i\rangle_{(4)}^{(\mathrm{prim})} - \langle\hat{T}_i\rangle_{(2)}^{(\mathrm{prim})}) \tag{22}$$

The motivation for eq 21 starts with the exact expression for the true fourth-order TI virial estimator

$$\langle\hat{T}_i\rangle_{(4)}^{(\mathrm{vir})} = \langle T_{\mathrm{TI},i}^{(\mathrm{vir})}(\{\mathbf{r}\}_i)w_{\mathrm{TI}}(\{\mathbf{r}\})\rangle_{(2)} \tag{23}$$

where $T_{\mathrm{TI},i}^{(\mathrm{vir})}(\{\mathbf{r}\}_i)$ is given by

$$T_{\mathrm{TI},i}^{(\mathrm{vir})}(\{\mathbf{r}\}_i) = \frac{3}{2\beta} + \frac{1}{2P}\sum_{k=1}^{P}(\mathbf{r}_i^{(k)} - \mathbf{r}_{\mathrm{c},i})\cdot\left(\frac{\partial V}{\partial \mathbf{r}_i^{(k)}} + \frac{\partial V_{\mathrm{TI}}}{\partial \mathbf{r}_i^{(k)}}\right) \tag{24}$$

If we now add and subtract $\langle T_i^{(\mathrm{vir})}(\{\mathbf{r}\})\rangle_{(2)}$ in eq 23, we obtain

$$\langle\hat{T}_i\rangle_{(4)}^{(\mathrm{vir})} = \langle T_i^{(\mathrm{vir})}(\{\mathbf{r}\}_i)\rangle_{(2)} + (\langle T_{\mathrm{TI},i}^{(\mathrm{vir})}(\{\mathbf{r}\}_i)w_{\mathrm{TI}}(\{\mathbf{r}\})\rangle_{(2)} - \langle T_i^{(\mathrm{vir})}(\{\mathbf{r}\}_i)\rangle_{(2)}) \tag{25}$$

which is an exact result. In order to avoid calculating $T_{\mathrm{TI},i}^{(\mathrm{vir})}(\{\mathbf{r}\})$, the ansatz we introduce is that of replacing the virial estimators in the term in brackets by their primitive counterparts, which is formally exact and leads to eq 21. The assumption in this ansatz is that the unfavorable fluctuations associated with primitive estimators are the same at second and fourth order and will, therefore, cancel in the subtraction, leading to an estimator that converges as smoothly as the second-order virial but with fourth-order accuracy. The quality of this new estimator needs to be tested, and we compare it to the other estimators in the Results section.

For an efficient thermodynamic integration, we wish to use as few λ points as possible. In the ideal case, the mass switching function $m(\lambda)$ would be such that the free energy derivative is constant over the whole range of λ. Such a switch function could in principle be designed, but that would require the knowledge of the free energy derivative in some parametrization, for example linear.[8] An alternative approach is to use a switching function that is physically motivated and ideally also applicable to a range of systems. Following a different formulation from that in ref 8, we construct $m_i(\lambda)$ so that it performs a linear switch of harmonic oscillator eigenenergies and satisfies the boundary conditions $m_i(0) = m_{i,0}$, $m_i(1) = m_{i,1}$. The motivation for the form of the switch is the free energy of a harmonic oscillator of frequency ω at temperature T

$$A = \frac{\hbar\omega}{2} + \frac{1}{\beta}\ln(1 - e^{-\beta\hbar\omega}) \tag{26}$$

dx.doi.org/10.1021/ct400911m | J. Chem. Theory Comput. 2014, 10, 1440−1453

The leading order term is $\hbar\omega/2$, and as $\omega \sim 1/\sqrt{m}$, a switch on the quantity $1/\sqrt{m}$ should be roughly linear and flat for nearly harmonic systems. Such a switch takes the form

$$\frac{1}{\sqrt{m}} = \frac{1-\lambda}{\sqrt{m_0}} + \frac{\lambda}{\sqrt{m_1}} \tag{27}$$

Solving for m, we obtain the following switching function:

$$m(\lambda) = \frac{m_0 m_1}{(\lambda\sqrt{m_0} + (1-\lambda)\sqrt{m_1})^2} \tag{28}$$

This switch should work well for very harmonic systems close to the ground state by construction, but the limits of its utility should be carefully tested. If the free energy derivative $dA/d\lambda$ using this switch is nearly flat, then it should be possible to perform an accurate thermodynamic integration with just one λ-point, namely the midpoint. An example of this mass switching function for boundary values of mass $m_0 = 1$ and $m_1 = 2$ is shown in Figure 1.

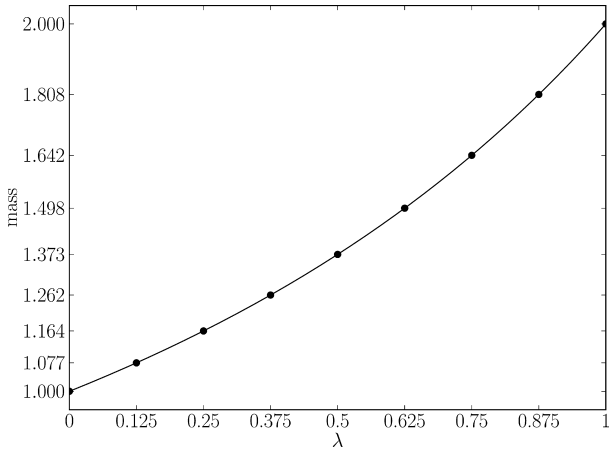

Figure 1. Plot of the mass switching function given by eq 28 for $m_0 = 1$, $m_1 = 2$. The nine values of λ used for thermodynamic integration in this work are marked on the axis.

3. COMPUTATIONAL DETAILS

Path-integral molecular dynamics simulations[24] of two model one-dimensional systems and four molecular systems were performed using an in-house implementation of the method. A transformation to staging variables,[25] together with a Nosé–Hoover chain thermostat,[24,26] attached to each path-integral degree of freedom was used to ensure efficient sampling of the canonical ensemble. The r-RESPA multiple time step method[27] was used to increase the accuracy of integration of the equations of motion while keeping the main time step as high as permitted by the physical interaction. All systems were simulated at nine different values of λ in the parametrization given by eq 28.

A harmonic oscillator system of mass m and spring constant k with a potential of the form

$$V(x) = \frac{1}{2}kx^2 \tag{29}$$

and the value of $k = 1$ was simulated at the temperature $T = 0.1$ for masses between $m_0 = 1$ and $m_1 = 2$. A total of 10^7 steps of length $\Delta t = 0.05$ were performed in each simulation, with 12 RESPA integration steps of the harmonic path integral interactions within each step of length Δt. A Nosé–Hoover chain of length three was coupled to each path integral degree of freedom. Reference values of the free energy derivative were calculated using the exact analytical formula obtained by differentiating eq 26 with respect to λ

$$\frac{dA}{d\lambda} = -\frac{1}{m}\frac{dm}{d\lambda}\langle\hat{T}\rangle = -\frac{1}{m}\frac{dm}{d\lambda}\frac{\hbar\omega}{4}\coth(\beta\hbar\omega/2) \tag{30}$$

where $\omega = (k/m)^{1/2}$.

A double-well system with a potential of the form

$$V(x) = \frac{D_0}{a^4}(x^2 - a^2)^2 \tag{31}$$

having parameter values of $D_0 = 2$ and $a = 0.5$ was simulated at the temperature $T = 1$ for masses between $m_0 = 1$ and $m_1 = 2$. For these parameters, the ground-state energy level for m_0 lies above the barrier while for m_1 it lies below the barrier. Hence, we expect qualitatively different behavior at these two mass values. A total of 4×10^6 steps of length $\Delta t = 0.01$ were performed in each simulation, with 20 RESPA integration steps of the harmonic path integral interactions within each step of length Δt. A Nosé–Hoover chain of length four was coupled to each path-integral degree of freedom. The number of path-integral beads P ranged from 4 to 256, increasing by a factor of 2. Reference values of the free energy derivative were obtained from a numerical solution of the Schrödinger equation in a sine basis on a finite interval. Convergence with respect to the number of basis functions was checked. The free energy derivative was calculated using eq 5, where the kinetic energy ensemble average was computed as a Boltzmann-weighted average of the kinetic energies of the eigenstates. Natural units ($k_B = 1$ and $\hbar = 1$) are used for the model systems.

Ab inito path-integral simulations[28] of the following molecular systems were performed: a water dimer, a protonated water dimer ($H_5O_2^+$), a deprotonated water dimer ($H_3O_2^-$), and a lithium cation microsolvated with four water molecules. All systems were simulated at a temperature $T = 300$ K to achieve thermal disorder and nuclear quantum effects comparable in magnitude to the condensed phase at ambient conditions. As was done in the model systems, staging variables were used. Each production simulation was 20 ps long following 1 ps of equilibration. The time step $\Delta t = 0.5$ fs was subdivided into 5 RESPA integration steps of the harmonic path integral interactions. A Nosé–Hoover chain of length 6 was attached to each path integral degree of freedom. Each thermostat integration step was further divided into multiple time steps with 2 RESPA steps and fourth-order Suzuki–Yoshida integration.[29,30] The thermostat time constant was set to $\tau = 20$ fs for the first path-integral bead and to the value of $\tau = 1/\omega_P$ for all the other beads for optimal sampling. Simulations were performed for values of P ranging from 4 to 32, increasing by a factor of 2. For the water dimer systems, all hydrogen nuclei were changed to deuterium nuclei. For the lithium system, the lithium cation was changed from the ^{6}Li isotope to the ^{7}Li isotope.

Interactions needed for path-integral molecular dynamics were evaluated using the MP2 method[31] as implemented in Gaussian 09 C.01[32] and obtained through the interface provided by the Atomic Simulation Environment.[33] Simulations of the neat, protonated, and deprotonated water dimers were carried out using both the 6-311++G** and 6-31+G* basis sets; whereas, simulations of the microhydrated lithium cation were carried out using the 6-31+G* basis set only.

Comparisons of path integral simulation results for the free energy difference to reference values were made using the signed percentage relative error of ΔA defined as

$$\delta\Delta A = 100\left(\frac{\Delta A}{\Delta A_{\mathrm{ref}}} - 1\right) \tag{32}$$

where ΔA_{ref} is a suitable reference value. Note that $\delta\Delta A$ can be either positive or negative. Thermochemical calculations were performed using Gaussian 09 C.01.[32]

In all of the studies to be presented, comparison of free energy derivatives is made between the second-order primitive estimators and the reweighting of these to obtain the fourth-order results. Although it would have been possible to use the full TI estimator for the model systems, we chose not to make such a comparison as the use of the full TI estimator is impractical in the ab initio applications studied here. A detailed error analysis of the different estimators using the technique of block averaging[34] is presented in the Supporting Information (SI), Figures S8−S11. The error analysis in the SI clearly shows that, although the error bars on the fourth-order reweighted estimators are larger at small P than they are for the second-order estimators, the second-order results at these small P values lie *outside* the error bars on the fourth-order estimators for most of the systems studied.

4. RESULTS

Here we present the free energy derivative $\mathrm{d}A/\mathrm{d}\lambda$ as well as the resulting free energy difference ΔA obtained using one to nine points for thermodynamic integration and all four estimators introduced in the Theory section. For the one-dimensional model systems, these results are also compared to the exact analytical or accurate numerical values. First, the convergence of the free energy derivative with respect to the number of path integral beads P must be investigated. To determine the number of beads needed for a given calculation, this convergence should be checked at the mass of the lighter isotope, as that is where quantum effects are the largest. Then, for a sufficient value of P, the dependence on λ determines the number of points needed to calculate the free energy difference between the two isotopes.

4.1. Model Systems. To investigate the properties of the proposed methods in detail and to compare to exact reference data, we simulated two model one-dimensional systems, a harmonic oscillator and a double well, using settings detailed in the previous section. We use natural units with $k_{\mathrm{B}} = 1$ and $\hbar = 1$ for these model systems. The convergence of the free energy derivative for the harmonic potential of eq 29 calculated using the four different estimators with respect to the number of path integral beads P is shown in Figure 2 for $\lambda = 0.0$ and 0.5. The exact result, computed analytically, is shown as the dashed black line. As expected, the values approach the exact result as P increases, but there are important differences between the methods. The behavior is essentially the same at $\lambda = 0.0$ and 0.5, with the $\lambda = 0.0$ point covering a wider range of values, as there are stronger quantum effects at lower mass. This confirms that convergence with P should be checked at the mass of the lighter isotope. Both the second- and fourth-order primitive estimators give the correct result, but given the trajectory length, they have noticeable sampling noise, especially for higher values of P. The Takahashi−Imada estimator converges faster, reaching the same value as the primitive estimator at roughly 2−3 times fewer beads. The virial estimator, on the other hand, is much better behaved with respect to sampling noise, due to its more favorable numerical properties. However, it is a second-order estimator, and it shows the same convergence behavior as the primitive second-order estimator. In order, therefore, to combine the advantages of both of these approaches—higher order estimation and smooth convergence of the virial estimator—we transfer the Takahashi−Imada correction to the virial estimator, eq 22. This result then converges as fast as the Takahashi−Imada estimator, yet has the low noise of the virial estimator. From the data for $\lambda = 0.0$, we can say that the value is certainly converged at $P = 64$. Therefore, we explore the λ dependence of the free energy derivative at this value of P.

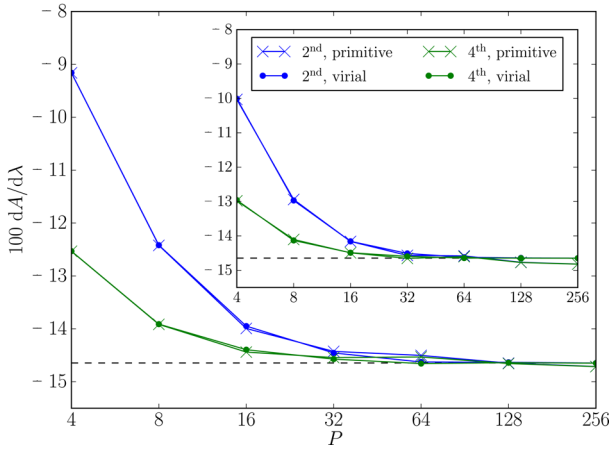

Figure 2. Convergence with respect to the number of path integral beads P of the free energy derivative $\mathrm{d}A/\mathrm{d}\lambda$ for the harmonic oscillator system, calculated using the four different estimators. The main panel shows data for $\lambda = 0.0$, and the inset shows data for $\lambda = 0.5$. Second-order estimators are shown in blue, and fourth-order estimators are shown in green. Primitive estimators are shown using crosses, and virial estimators are shown using full circles. Lines are provided to guide the eye. The exact analytical value (independent of P) is shown for reference using a black dashed line.

The result is shown in Figure 3, both in detail and on the full scale from zero, which is important for the subsequent thermodynamic integration. Thanks to the mass switching function used, the values are essentially constant across the whole range of λ. The detailed view in the inset reveals some differences between the four estimators, which are, however, negligible for this system at this value of P. We can see a very small remaining error of the second-order estimators and the larger variation of the primitive estimators compared to the virial ones. This can be compared to the same result with a linear switching function, shown in the bottom panel of Figure 1 in ref 35, where the free energy derivative changes by a factor of more than 2.5. It is clear that thermodynamic integration of the free energy derivative to obtain the free energy difference between the two isotopes does not need many λ points to converge. Figure 4 illustrates this point in detail. The error of the resulting free energy difference is in fact constant with the number of points, and any remaining deviation from the exact result is very small (less than 0.5%). Thus, *a single point at $\lambda = 0.5$ is sufficient to calculate the full free energy difference.* Numerical values for the reference and for PIMD with nine thermodynamic integration points are summarized in Table 1. These results for the harmonic oscillator system are very promising, but before the methodology can be deemed useful in practice, it must be checked that it performs comparably well

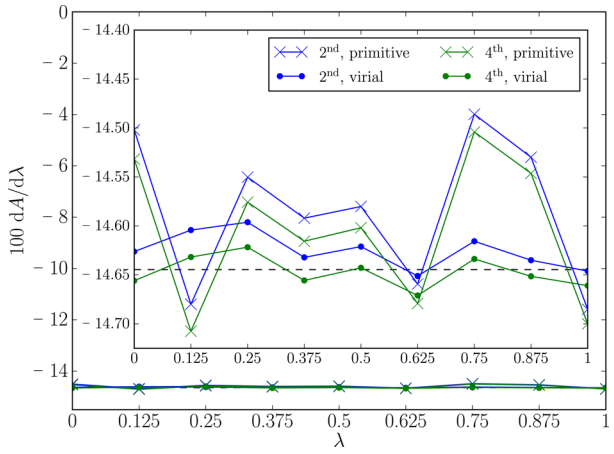

Figure 3. Dependence of the free energy derivative $dA/d\lambda$ on λ in the parametrization given by eq 28 for the harmonic oscillator system, calculated using the four different estimators. 64 path integral beads and 9 evenly spaced λ points are used. The inset shows the details of the same data. Second-order estimators are shown in blue, and fourth-order estimators are shown in green. Primitive estimators are shown using crosses, and virial estimators are shown using full circles. Lines are provided to guide the eye. The exact analytical value is shown for reference using a black dashed line.

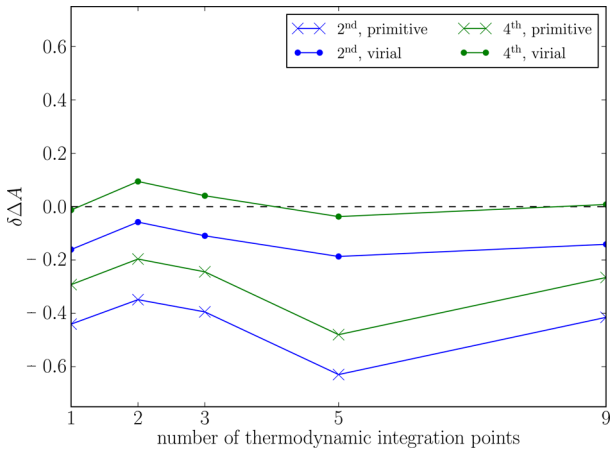

Figure 4. Dependence of the free energy difference percentage error $\delta\Delta A$ (eq 32) on the number of points used in thermodynamic integration for the harmonic oscillator system. The exact value is used as reference. 64 path integral beads are used. Second-order estimators are shown in blue, and fourth-order estimators are shown in green. Primitive estimators are shown using crosses, and virial estimators are shown using full circles. Lines are provided to guide the eye.

Table 1. Free Energy Differences for the Harmonic Oscillator System Obtained Using the Different Methods[a]

method	1-point TI ΔA	9-point TI ΔA	exact ΔA
exact			−0.14645
primitive 2nd order	−0.14580	−0.14584	
virial 2nd order	−0.14621	−0.14606	
primitive Takahashi−Imada	−0.14613	−0.14624	
virial Takahashi−Imada	−0.14654	−0.14646	

[a]The PIMD data uses 64 beads and 1 or 9 thermodynamic integration points.

for more challenging systems. Importantly, the nearly constant shift between the second and fourth order primitive estimators seen in Figure 3 as a function of λ provides insight into the advantage of the proposed estimator in eq 22. By reweighting the configurations generated at second-order as an a posteriori procedure, the nearly constant difference between the second- and fourth-order primitive estimators approximates the fourth-order correction to the second virial estimator.

As the mass switching function that we use is motivated by the dependence of energy eigenvalues of a harmonic oscillator on mass, it is important to investigate its performance for strongly anharmonic systems. To do this, we simulated a one-dimensional double well system with potential energy given by eq 31. Convergence of the free energy derivate is shown in Figure 5 and has the same characteristics as in the case of the

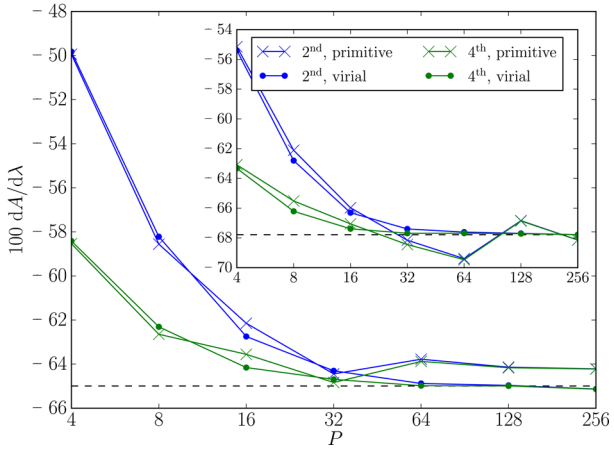

Figure 5. Convergence with respect to the number of path integral beads P of the free energy derivative $dA/d\lambda$ for the double well system, calculated using the four different estimators. Main panel: data for λ = 0.0; Inset: data for λ = 0.5. Second-order estimators are shown in blue, and fourth-order estimators are shown in green. Primitive estimators are shown using crosses, and virial estimators are shown using full circles. Lines are provided to guide the eye. The numerical reference value (independent of P) is shown using a black dashed line.

harmonic oscillator system above. Even though sampling error in the primitive estimators is worse than for the harmonic oscillator system, both virial estimators still perform well and converge smoothly to the accurate numerical reference value. The fourth-order virial, for example, gives a value for ΔA of −0.68469, which compares well to the reference value of −0.68504. Using 64 beads as the converged value of P, we can investigate the λ dependence, which is shown in Figure 6. Although the deviation from a constant value is noticeable in this case, it is still rather small compared to the magnitude of the free energy derivative. More importantly, the deviation from linearity is very small, which suggests that thermodynamic integration using only a few points should still perform well. However, the relevant criterion is the resulting value of the free energy difference. As before, Figure 7 shows the percentage error of ΔA relative to the reference value. Again, the error is very small even for a single thermodynamic integration point, with improved convergence as the number of points is increased. We can see that the use of a single simulation for which λ = 0.5 is an excellent approximation even in this strongly anharmonic system. The reason that even a single λ-point, here λ = 0.5, can be used is the fact that $dA/d\lambda$ is approximately linear and symmetric about this point. Interestingly, at a particular temperature, specifically T = 0.625, the free energy derivative becomes nonmonotomic. For

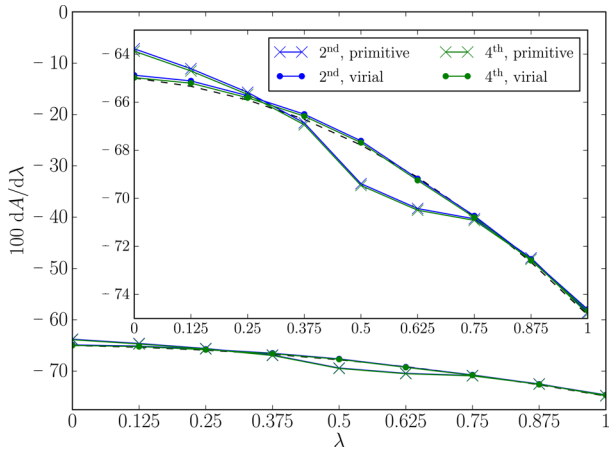

Figure 6. Dependence of the free energy derivative $dA/d\lambda$ on λ in the parametrization given by eq 28 for the double well system, calculated using the four different estimators. 64 path integral beads and 9 evenly spaced λ points are used. Inset: detail of the same data. Second-order estimators are shown in blue, and fourth-order estimators are shown in green. Primitive estimators are shown using crosses, and virial estimators are shown using full circles. Lines are provided to guide the eye. The numerical reference value (independent of P) is shown using a black dashed line.

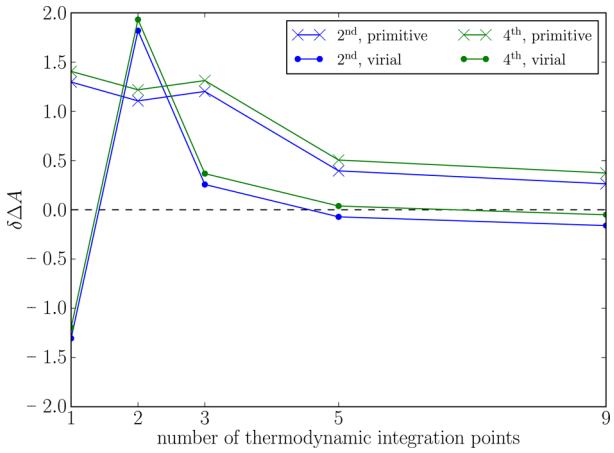

Figure 7. Dependence of the free energy difference percentage error $\delta\Delta A$ (eq 32) on the number of points used in thermodynamic integration for the double-well system. The exact numerical value is used as reference. 64 path integral beads are used. Second-order estimators are shown in blue, and fourth-order estimators are shown in green. Primitive estimators are shown using crosses, and virial estimators are shown using full circles. Lines are provided to guide the eye.

such a system, one might expect that more thermodynamic integration points are needed. This issue is explored in more detail in the SI, Figures S1−S3.

4.2. Water Dimer. To move to practical application of the proposed methodology, we investigate isotopic substitution in the water dimer and its protonated and deprotonated variants, namely, the proton transfer complexes $H_5O_2^+$ and $H_3O_2^-$, respectively, using ab initio path-integral molecular dynamics. Note that the $H_5O_2^+$ complex is the well-known "Zundel" cation, while the $H_3O_2^-$ can be viewed as the negative analog of a Zundel-like complex. In all three cases, we substitute all hydrogen nuclei for deuterium nuclei. Recent path integral molecular dynamics studies of $H_5O_2^+$ and its isotopomers found that the tempearture dependence of structural fluctuations were greater for $D_5O_2^+$ than for $H_5O_2^+$.[36] Simulations of these systems were performed using interactions at the MP2 level of theory with both the 6-311++G** and 6-31+G* basis sets. The results are qualitatively the same, and quantitatively the free energy differences vary by only about 1%. In the following, we show results obtained with the larger basis set only.

The convergence of the free energy derivative at $\lambda = 0.0$ with respect to the number of path integral beads P for the neat water dimer is shown in Figure 8. While we do not see perfect

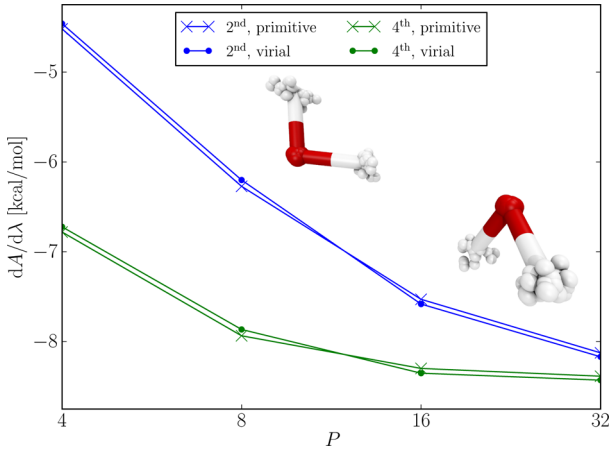

Figure 8. Convergence with respect to the number of path integral beads P of the free energy derivative $dA/d\lambda$ for the water dimer at $\lambda = 0.0$, calculated using the four different estimators. Second-order estimators are shown in blue, and fourth-order estimators are shown in green. Primitive estimators are shown using crosses, and virial estimators are shown using full circles. A typical snapshot from the simulation at $P = 32$ is shown for illustration. Lines are provided to guide the eye.

saturation in the range of values explored, it is clear that the fourth order estimators allow the use of substantially fewer beads. We use the value $P = 16$ for further analysis, as at fourth order it differs by less than 1% from the value at $P = 32$ and is closer to the converged value than the second-order estimator at $P = 32$. Although $P = 16$ does not fully converge the second-order estimators, it is still instructive to compare the convergence with respect to the number of λ points, as the difference from the corresponding fourth-order values is an approximately constant offset. We estimated that the second order estimators would be fully converged around $P = 64$. We next focus on the dependence of the free energy derivative on λ for the neat water dimer, which is shown in Figure 9. We can see that although it is not entirely constant, it is linear to a very good approximation. As before, the data based on the second order virial estimator shows less noise and the transfer of the fourth order correction to it works well. The free energy derivatives of the other two systems are analogous but scaled in magnitude due to the different number of hydrogen nuclei in these systems. The P convergence data is shown in Figures S4 and S6 of the SI, and the λ dependence data is shown in Figures S5 and S7 of the SI.

In the case of the $H_5O_2^+$ and $H_3O_2^-$ complexes, there are two nonequivalent hydrogen nuclei in the system—the central one shared by the oxygen atoms and the either two or four dangling ones. Their contributions to the total free energy difference are not the same, indicating different nuclear

dx.doi.org/10.1021/ct400911m | J. Chem. Theory Comput. 2014, 10, 1440−1453

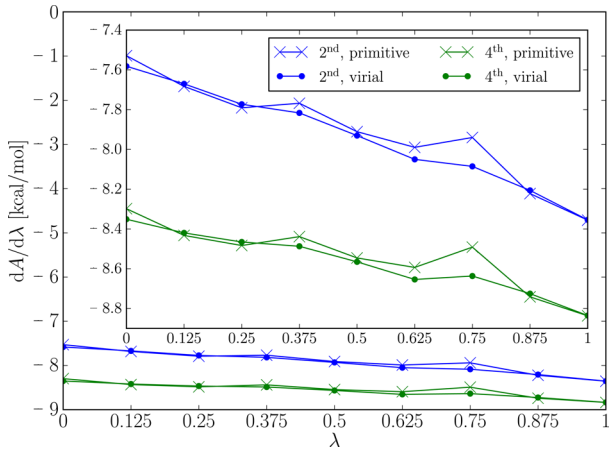

Figure 9. Dependence of the free energy derivative $dA/d\lambda$ on λ in the parametrization given by eq 28 for the water dimer, calculated using the four different estimators. Sixteen path integral beads and 9 evenly spaced λ points are used. Inset: detail of the same data. Second-order estimators are shown in blue, and fourth-order estimators are shown in green. Primitive estimators are shown using crosses, and virial estimators are shown using full circles. Lines are provided to guide the eye.

quantum effects for these positions. In the case of the $H_3O_2^-$ complex, the central proton contributes about 82% of the free energy contributed by each dangling bond, averaged over the dangling bonds. In the protonated case, this ratio is about 79%.

To assess the quality of the resulting free energy difference ΔA, we examine the percent relative error of eq 32, with the value of ΔA obtained from the virial Takahashi–Imada estimator using nine thermodynamic integration points as the reference. This error, as a function of the number of thermodynamic integration points used, is shown for the three variants of the system and for the four different estimators in Figures 10, 11, and 12. In all cases, the error of the virial Takahashi–Imada estimator is very small, remaining below

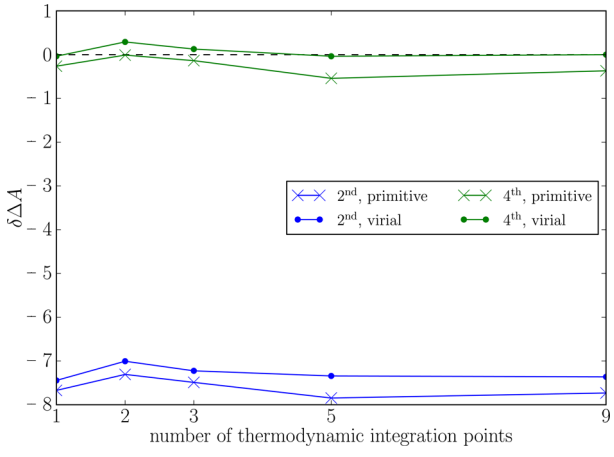

Figure 10. Dependence of the free energy difference percentage error $\delta\Delta A$ (eq 32) on the number of points used in thermodynamic integration for the water dimer. The value calculated using the Takahashi–Imada virial estimator and nine thermodynamic integration points is used as reference. Sixteen path-integral beads are used. Second-order estimators are shown in blue, and fourth-order estimators are shown in green. Primitive estimators are shown using crosses, and virial estimators are shown using full circles. Lines are provided to guide the eye.

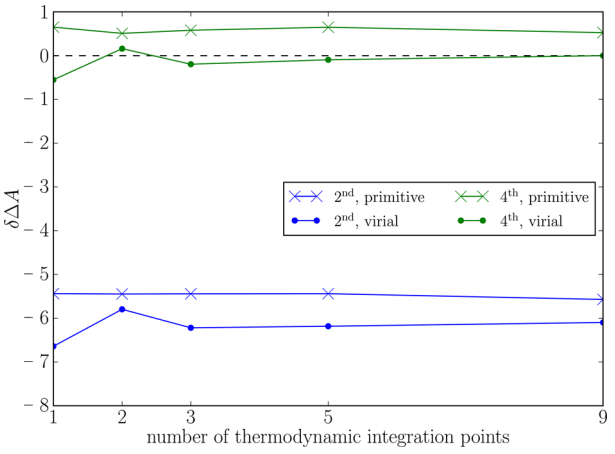

Figure 11. Dependence of the free energy difference percentage error $\delta\Delta A$ (eq 32) on the number of points used in thermodynamic integration for the protonated water dimer. The value calculated using the Takahashi–Imada virial estimator and nine thermodynamic integration points is used as reference. Sixteen path integral beads are used. Second-order estimators are shown in blue, and fourth-order estimators are shown in green. Primitive estimators are shown using crosses, and virial estimators are shown using full circles. Lines are provided to guide the eye.

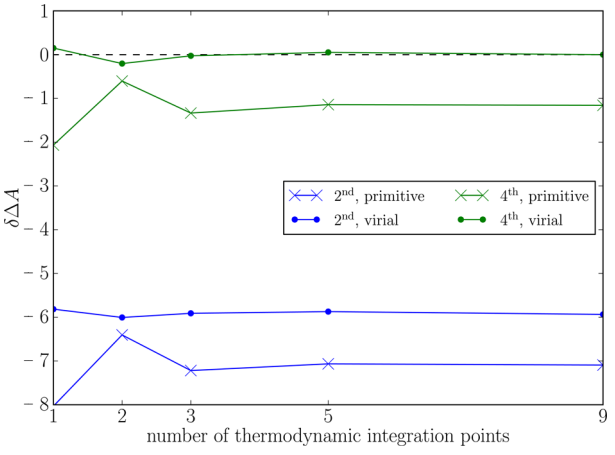

Figure 12. Dependence of the free energy difference percentage error $\delta\Delta A$ (eq 32) on the number of points used in thermodynamic integration for the deprotonated water dimer. The value calculated using the Takahashi–Imada virial estimator and nine thermodynamic integration points is used as reference. Sixteen path integral beads are used. Second-order estimators are shown in blue, and fourth-order estimators are shown in green. Primitive estimators are shown using crosses, and virial estimators are shown using full circles. Lines are provided to guide the eye.

0.5% over the whole range. Although the error is often larger at a lower number of points, this can be attributed to more sampling noise. The data for second order estimators is offset by a constant due to the incomplete convergence with respect to the number of beads P, but the convergence of the thermodynamic integration is equally fast.

Numerical values of free energy differences obtained using the fourth-order estimators and nine thermodynamic integration points for all three water dimer systems are shown in Table 2. For comparison, we have also performed thermochemical calculations for these systems based on frequency analysis in the global minimum of the potential energy hypersurface. As the numbers in Table 2 show, this approach overestimates the

Table 2. Free Energy Differences for the Three Water Dimer Variants Obtained Using Thermochemistry and the Fourth-Order Estimators, Sixteen Path-Integral Beads, and One or Nine Thermodynamic Integration Points

method	ΔA [kcal/mol]		
	$(H_2O)_2$	$H_5O_2^+$	$H_3O_2^-$
thermochemistry	−8.894	−10.547	−5.882
primitive Takahashi−Imada, 1-point TI	−8.546	−10.414	−5.568
primitive Takahashi−Imada, 9-point TI	−8.537	−10.401	−5.620
virial Takahashi−Imada, 1-point TI	−8.565	−10.290	−5.694
virial Takahashi−Imada, 9-point TI	−8.568	−10.347	−5.686

magnitude of the free energy difference by about 3%. Although this is a relatively good result given the lower computational cost, we note that it should not be relied on in general. Even for these small systems, there are low-frequency modes which the method cannot describe reliably. For larger or condensed-phase systems, such a calculation would be entirely impossible.

4.3. Microhydrated Lithium Cation. The last system chosen to test the methodology is a molecular cluster that is interesting from an applications point of view and which is also computationally more challenging. We microsolvated a lithium cation with its first hydration shell of four water molecules and calculated the free energy difference upon the substitution of ^{6}Li for ^{7}Li. While this approach does not include the hydration effects of an extended environment, it does describe the strong local interactions with high accuracy. The atom undergoing isotope exchange does not participate in any covalent bonds but, rather, moves in an effective strongly anharmonic potential created by the hydrating water molecules. Because the smaller basis set proved sufficient for the water dimer systems and the lithium cation is electronically very hard, we chose to conduct the simulations of this system with interactions at the MP2/6-31+G* level only. Convergence of the free energy derivative with respect to the number of path integral beads P is shown in Figure 13. The change with increasing P is substantially smaller compared to the water dimer case, suggesting a smaller magnitude of nuclear quantum effects. We chose $P = 16$ as the number of beads for calculations at multiple values of λ. Figure 14 shows the λ dependence of the free energy derivative. As in the example of the water dimer, the derivative for this system is also linear with respect to λ and remains much closer to a constant over the full λ range. With the current trajectory lengths, there is also considerable noise, especially in the primitive estimators, and the difference between the second- and fourth-order primitive estimator is not as smooth as the second-order virial estimator. Looking at the error of the free energy difference obtained by thermodynamic integration of an increasing number of points in Figure 15, we can see that both

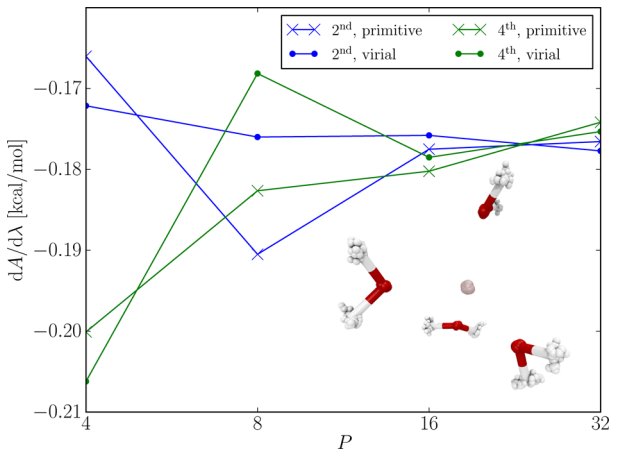

Figure 13. Convergence with respect to the number of path integral beads P of the free energy derivative $dA/d\lambda$ for the microhydrated lithium cation at $\lambda = 0.0$, calculated using the four different estimators. Second-order estimators are shown in blue, and fourth-order estimators are shown in green. Primitive estimators are shown using crosses, and virial estimators are shown using full circles. A typical snapshot from the simulation at $P = 32$ is shown for illustration. Lines are provided to guide the eye.

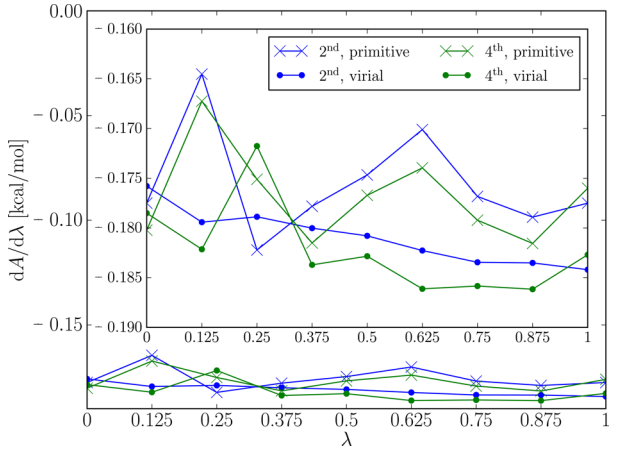

Figure 14. Dependence of the free energy derivative $dA/d\lambda$ on λ in the parametrization given by eq 28 for the microhydrated lithium cation, calculated using the four different estimators. Sixteen path integral beads and nine evenly spaced λ points are used. Inset: detail of the same data. Second-order estimators are shown in blue, and fourth-order estimators are shown in green. Primitive estimators are shown using crosses, and virial estimators are shown using full circles. Lines are provided to guide the eye.

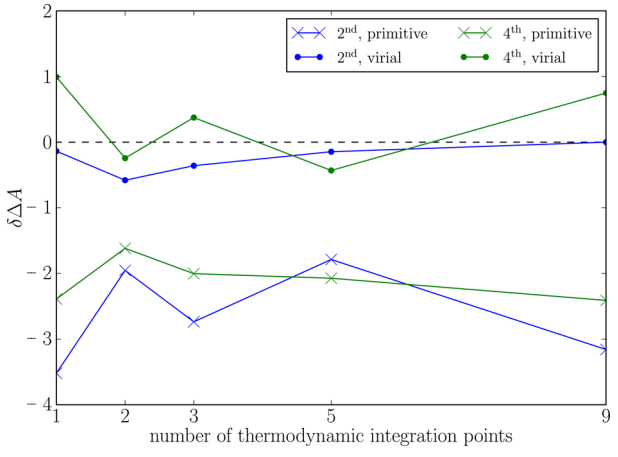

Figure 15. Dependence of the free energy difference percentage error $\delta\Delta A$ (eq 32) on the number of points used in thermodynamic integration for the microhydrated lithium cation. The value calculated using the virial estimator and nine thermodynamic integration points is used as reference. Sixteen path integral beads are used. Second-order estimators are shown in blue, and fourth-order estimators are shown in green. Primitive estimators are shown using crosses, and virial estimators are shown using full circles. Lines are provided to guide the eye.

dx.doi.org/10.1021/ct400911m | J. Chem. Theory Comput. 2014, 10, 1440−1453

virial estimators are converged to within 1% using the midpoint only, with no obvious convergence as the number of thermodynamic integration points is increased. Numerical values of the free energy difference for the exchange of ^{6}Li for ^{7}Li using the virial second- and fourth-order estimators computed from a nine-point thermodynamic integration are −0.181 and −0.182 kcal/mol, respectively, at this level of theory. At the same level of theory, the thermochemical result is −0.188 kcal/mol. It should be noted, however, that the agreement is likely fortuitous, as the harmonic approximation is known to be unreliable for weakly bound systems with many soft modes.

4.4. Discussion. The results generally show the advantage of the primitive Takahashi−Imada estimator of the quantum kinetic energy when compared to the usual second order estimator. On the other hand, it is also clear that this fourth-order estimator suffers from the same numerical problem as the second-order estimator—they are both primitive estimators containing the highly fluctuating harmonic interaction energy of the path integral ring polymer. In principle, this problem can be overcome by increasing trajectory length until the error of these estimators becomes acceptable. In practice, however, this can easily become prohibitively expensive, especially in the case of AIPIMD. Taking the difference between the averages of the second- and fourth-order estimator over the same ensemble produces a fourth-order correction to kinetic energy. As expected, our data shows that this correction does not suffer from the large fluctuations of the primitive estimators, as they cancel out to a large degree. The second-order virial estimator converges much faster than the primitive estimators with increased sampling and shows little noise in the above simulation results. To combine the advantage of fourth-order convergence with the number of path integral beads and the stability of the virial estimator, we add the fourth-order correction to the kinetic energy calculated using the virial estimator. The resulting estimator shows reasonable behavior with our data. This approach could in principle be used for estimators of other quantities as well, although we have not explored that in this work. Our primitive estimator data for both model systems are noticeably influenced by noise, especially in the case of the double well system. Although we could run these inexpensive calculations long enough to beat the fluctuations, we chose to show the data as presented in order to illustrate the difference between the two types of estimators. Using the coordinate scaling technique of Yamamoto,[37] a fourth-order virial estimator for the quantum kinetic energy could possibly be constructed. This method, however, uses a finite difference calculation and thus requires another evaluation of physical interactions for each contribution to ensemble averages. This represents substantial computational cost for ab initio calculations. Given the existence of an alternative in form of the above fourth-order correction, we have not pursued this further.

The λ dependence of the free energy derivative exhibits excellent behavior under thermodynamic integration using only a few points for all the systems studied here. In fact, in most practical applications, a single point at $\lambda = 0.5$ is sufficient to calculate the free energy difference between the two isotopes. Even in the rather specific case of a microsolvated lithium cation, with no covalent bonds and a strongly anharmonic effective potential, the midpoint serves as an excellent estimate of the full free energy difference.

The error caused by the use of the midpoint only as opposed to the use of nine points for thermodynamic integration is comparable to several other sources of error that are necessarily present. The difference between the results obtained using the two basis sets tested for the water dimer is about 1%. In general, with any electronic structure method or empirical force field the approximations or the difference between several methods will introduce an error in the final free energy difference ΔA. For the water dimer systems, although we have used $P = 16$ for our calculations, the convergence tests show that even with fourth-order estimators, there remains a small difference between the free energy derivative at $P = 16$ and $P = 32$ of about 1%. This will translate to a comparable error in ΔA almost directly, due to the thermodynamic integration scheme and the similar P convergence behavior at different values of λ. Sampling error will depend very much on the specific application but could easily dominate, particularly for AIPIMD. Given all these contributions, the small error introduced by the approximate thermodynamic integration using only the midpoint is entirely acceptable.

Although the switch function was motivated by harmonic systems, it works even in anharmonic cases. This can be understood by looking at the plots of the free energy derivative as a function of λ. Even if it does deviate from a constant, it is really the deviation from linearity that determines the error as a function of the number of thermodynamic integration points. Note that due to the curvature of the free energy derivative, the error when using the two end points can be larger than the error using the midpoint only, as is observed for the double-well model system.

The second derivative of free energy with respect to λ, derived in the Appendix, could in principle be used in a thermodynamic integration scheme. This would, however, require an efficient estimator of $\langle \hat{T}^2 \rangle$, preferably one that converges as well as our virial Takahashi−Imada estimator for $\langle \hat{T} \rangle$. Because our approach based on the first derivative already works rather well, it could happen that a poorly converged $\langle \hat{T}^2 \rangle - \langle \hat{T} \rangle^2$ (either with respect to P or in terms of sampling) could in fact degrade the result. As fluctuations are known to be more demanding in terms of the amount of sampling required, we have not attempted to make use of the second derivative in the present study.

Pérez and von Lilienfeld[35] performed calculations using a linear mass switching function for both the harmonic oscillator (their Figure 1, bottom panel) and the protonated water dimer, using density functional theory, second-order estimators, and five thermodynamic integration points (their Figure 3). In both cases, the free energy derivative changes by at least a factor of 2 between the two isotopes. A comparison of these results to our results in Figures 3 and S2, where the value changes very little over the whole range, illustrates the importance of the choice of the mass switching function.

Ceriotti and Markland[8] proposed, among others, two different estimators for the quantum kinetic energy based on free energy perturbation—a thermodynamic reweighting one (TD-FEP) and one based on the coordinate scaling approach of Yamamoto[37] (SC-FEP). Although SC-FEP has more favorable numerical properties, as discussed above, it requires an additional evaluation of physical interactions, increasing substantially the cost of ab initio simulations. On the other hand, free energy perturbation calculations are very efficient in situations where many different equivalent atoms can

contribute, which is the case for hydrogen/deuterium fractionation and liquid water, for example.

5. CONCLUSIONS

In this paper, we propose a combination of methods that allows efficient calculation of free energy differences upon isotope substitution using path integral molecular dynamics. In order to decrease the number of path integral beads, we use the Takahashi–Imada fourth-order estimator of the quantum kinetic energy. We avoid the problem of sampling noise in this estimator by extracting a correction from the second- and fourth-order estimators and adding it to the numerically more favorable second-order virial estimator. This new estimator is especially suitable for ab initio calculations, as it requires neither additional evaluations of interactions nor second derivatives of the interaction potential. We recognize that the reweighting used in the fourth-order scheme could become inefficient for large systems as suggested by Ceriotti et al.[41] The limit at which this occurs, however, merits further investigation.

In order to improve the efficiency of the calculations even further, we employ a thermodynamic integration scheme based on a mass switching function motivated by the behavior of purely harmonic systems (see eq 28). The combination of the new switching function and fourth-order free energy derivative estimators was applied to the toy examples of the harmonic oscillator and the double well potential and to model protonated ($H_5O_2^+$), neutral (H_4O_2), and deprotonated ($H_3O_2^-$) water dimer systems as well as the microsolvated lithium cation. This switch is shown to perform well for atoms in covalent bonds, which are present in the water dimer problems, and allows the calculation of the full free energy difference using a single simulation at $\lambda = 0.5$. Even in the special case of a light atom with no covalent bonds, which occurs in the microsolvated lithium cation example, a single-point thermodynamic integration approach with the switch in eq 28 provides a practically converged result.

Going forward, several additional enhancements of the methodology will be investigated. First, the single-point thermodynamic integration approach could be combined with free energy perturbation calculations from the midpoint to the end points. It should be possible to design an optimal formulation of such an approach that could both reduce errors and improve the efficiency of the calculations, particularly in condensed-phase systems. Second, the possibility of devising fourth-order virial estimators for observables other than the free energy derivative based on the idea presented in eq 21 will be explored. Given the improvements seen here in the convergence properties of such estimators, this would constitute an important advance in path integral methodology.

APPENDIX: FREE ENERGY DERIVATIVES

In this appendix, we derive expressions for the first and second λ derivatives of the free energy from the path-integral expression. For simplicity, consider the partition function for a single particle

$$Q(\lambda) = \left(\frac{m(\lambda)P}{2\pi\beta\hbar^2}\right)^{3P/2} \int \mathrm{d}\mathbf{r}_1 \ldots \mathrm{d}\mathbf{r}_P \mathrm{e}^{-\beta V_{\mathrm{eff}}(\{\mathbf{r}\},\lambda)} \tag{A.1}$$

where $V_{\mathrm{eff}}(\{\mathbf{r}\})$ is the effective potential corresponding to a particlar approximation to the high-temperature imaginary-time propagator. The free energy profile in λ is

$$A(\lambda) = -\frac{1}{\beta}\ln Q(\lambda) \tag{A.2}$$

Thus

$$\frac{\mathrm{d}A}{\mathrm{d}\lambda} = -\frac{1}{\beta Q(\lambda)}\frac{\partial Q}{\partial \lambda}$$
$$\frac{\mathrm{d}^2A}{\mathrm{d}\lambda^2} = \frac{1}{\beta}\left[\left(\frac{1}{Q(\lambda)}\frac{\partial Q}{\partial \lambda}\right)^2 - \frac{1}{Q(\lambda)}\frac{\partial^2 Q}{\partial \lambda^2}\right] \tag{A.3}$$

Taking the first derivative of $Q(\lambda)$, we obtain

$$\frac{1}{Q}\frac{\partial Q}{\partial \lambda} = \frac{3P}{2}\frac{m'(\lambda)}{m(\lambda)} - \beta\left\langle \frac{\partial V_{\mathrm{eff}}}{\partial \lambda}\right\rangle \tag{A.4}$$

while the second derivative yields

$$\frac{1}{Q}\frac{\partial^2 Q}{\partial \lambda^2} = \frac{3P}{2}\left[\frac{m''(\lambda)}{m(\lambda)} - \left(\frac{m'(\lambda)}{m(\lambda)}\right)^2\right] + \frac{3P}{2}\frac{m'(\lambda)}{m(\lambda)}$$
$$\left[\frac{3P}{2}\frac{m'(\lambda)}{m(\lambda)} - \beta\left\langle \frac{\partial V_{\mathrm{eff}}}{\partial \lambda}\right\rangle\right] - \frac{3P\beta}{2}\frac{m'(\lambda)}{m(\lambda)}\left\langle \frac{\partial V_{\mathrm{eff}}}{\partial \lambda}\right\rangle$$
$$- \beta\left\langle\left[\frac{\partial^2 V_{\mathrm{eff}}}{\partial \lambda^2} - \beta\left(\frac{\partial V_{\mathrm{eff}}}{\partial \lambda}\right)^2\right]\right\rangle \tag{A.5}$$

Substituting eqs A.4 and A.5 into eq A.3 and simplifying, we obtain the following expression for the second derivative in terms of a particular V_{eff}:

$$\frac{\mathrm{d}^2A}{\mathrm{d}\lambda^2} = \frac{3P}{2\beta}\left(\frac{m'(\lambda)}{m(\lambda)}\right)^2 - \frac{3P}{2\beta}\frac{m''(\lambda)}{m(\lambda)}$$
$$- \beta\left[\left\langle \frac{\partial V_{\mathrm{eff}}}{\partial \lambda}\right\rangle^2 - \left\langle \frac{\partial V_{\mathrm{eff}}}{\partial \lambda}\right\rangle^2\right] + \left\langle \frac{\partial^2 V_{\mathrm{eff}}}{\partial \lambda^2}\right\rangle \tag{A.6}$$

Now consider the second-order effective potential in eq 9:

$$V_{\mathrm{eff}}^{(2)}(\{\mathbf{r}\}, \lambda) = \frac{1}{2}m(\lambda){\omega_P}^2\sum_{k=1}^{P}(\mathbf{r}_{k+1} - \mathbf{r}_k)^2 + \frac{1}{P}\sum_{k=1}^{P}V(\mathbf{r}_k) \tag{A.7}$$

From this potential, we have

$$\frac{\partial V_{\mathrm{eff}}^{(2)}}{\partial \lambda} = \left(\frac{m'(\lambda)}{m(\lambda)}\right)\frac{1}{2}m(\lambda){\omega_P}^2\sum_{k=1}^{P}(\mathbf{r}_{k+1} - \mathbf{r}_k)^2$$
$$= \frac{m'(\lambda)}{m(\lambda)}\left(\frac{3P}{2\beta} - T^{(\mathrm{prim})}\right)$$
$$\frac{\partial^2 V_{\mathrm{eff}}^{(2)}}{\partial \lambda^2} = \left(\frac{m''(\lambda)}{m(\lambda)}\right)\frac{1}{2}m(\lambda){\omega_P}^2\sum_{k=1}^{P}(\mathbf{r}_{k+1} - \mathbf{r}_k)^2$$
$$= \frac{m''(\lambda)}{m(\lambda)}\left(\frac{3P}{2\beta} - T^{(\mathrm{prim})}\right) \tag{A.8}$$

Substituting this into eq A.6 and simplifying, we obtain

$$\frac{\mathrm{d}^2A}{\mathrm{d}\lambda^2} = -\beta\left(\frac{m'(\lambda)}{m(\lambda)}\right)^2\left[\langle (T^{(\mathrm{prim})})^2\rangle - \langle T^{(\mathrm{prim})}\rangle^2 - \frac{3P}{2\beta^2}\right]$$
$$- \frac{m''(\lambda)}{m(\lambda)}\langle T^{(\mathrm{prim})}\rangle \tag{A.9}$$

dx.doi.org/10.1021/ct400911m | J. Chem. Theory Comput. 2014, 10, 1440–1453

Equation A.9 shows that computing the second derivative of the free energy with respect to λ requires computing the kinetic energy fluctuations, which are slow to converge due to statistical noise. The presence of $-3P/(2\beta^2)$ in the first term is expected, since the fluctuations are those of the primitive kinetic energy estimator, which, as was shown by Herman et al.,[17] grow linearly with P. This estimator could be converted into a virial form following a procedure similar to that employed by Glaeserman and Fried in their derivation of a heat-capacity estimator;[38] however, such an estimator would involve the Hessian, which is problematic, particularly for ab initio path-integral calculations. Note that an expression for the second derivative of the free energy with respect to λ was presented in ref 35; however, it appears as if the authors missed the term involving these kinetic energy fluctuations. Given the dependence of this derivative on these fluctuations, it is not clear if constructing the free energy profile using second-derivative data will improve the accuracy of the overall result, and this is something that merits further investigation. Finally, it is straightforward, if tedious, to extend eq A.9 for mass changes of multiple particles. The resulting expression for $d^2A/d\lambda^2$ will involve fluctuations in appropriate sums of primitive kinetic energy estimators together with their corresponding mass derivative factors, and the same slow convergence issues will apply.

Next, consider the fourth-order effective potential

$$V_{\mathrm{eff}}^{(4)}(\{\mathbf{r}\},\lambda) = \frac{1}{2}m(\lambda){\omega_P}^2\sum_{k=1}^{P}(\mathbf{r}_{k+1}-\mathbf{r}_k)^2 + \frac{1}{P}\sum_{k=1}^{P}V(\mathbf{r}_k) + \frac{1}{24P^2{\omega_P}^2m(\lambda)}\sum_{k=1}^{P}\left(\frac{\partial V}{\partial \mathbf{r}_k}\right)^2 \tag{A.10}$$

The λ derivatives of this potential are

$$\frac{\partial V_{\mathrm{eff}}^{(4)}}{\partial\lambda} = \left(\frac{m'(\lambda)}{m(\lambda)}\right)\frac{1}{2}m(\lambda){\omega_P}^2\sum_{k=1}^{P}(\mathbf{r}_{k+1}-\mathbf{r}_k)^2 - \frac{m'(\lambda)}{24P^2{\omega_P}^2m^2(\lambda)}\sum_{k=1}^{P}\left(\frac{\partial V}{\partial \mathbf{r}_k}\right)^2 = \frac{m'(\lambda)}{m(\lambda)}\left(\frac{3P}{2\beta}-T_{\mathrm{TI}}^{(\mathrm{prim})}\right)$$

$$\frac{\partial^2 V_{\mathrm{eff}}^{(4)}}{\partial\lambda^2} = \left(\frac{m''(\lambda)}{m(\lambda)}\right)\frac{1}{2}m(\lambda){\omega_P}^2\sum_{k=1}^{P}(\mathbf{r}_{k+1}-\mathbf{r}_k)^2 - \left[\frac{m''(\lambda)}{m(\lambda)}-2\left(\frac{m'(\lambda)}{m(\lambda)}\right)^2\right]\frac{1}{24P^2{\omega_P}^2m(\lambda)}\sum_{k=1}^{P}\left(\frac{\partial V}{\partial \mathbf{r}_k}\right)^2 = \frac{m''(\lambda)}{m(\lambda)}\left(\frac{3P}{2\beta}-T_{\mathrm{TI}}^{(\mathrm{prim})}\right)+2\left(\frac{m'(\lambda)}{m(\lambda)}\right)^2 V_{\mathrm{TI}}(\{\mathbf{r}\}) \tag{A.11}$$

Substituting this result into eq A.6 yields the result

$$\frac{d^2A}{d\lambda^2} = -\beta\left(\frac{m'(\lambda)}{m(\lambda)}\right)^2\left[\langle(T_{\mathrm{TI}}^{(\mathrm{prim})})^2\rangle - \langle T_{\mathrm{TI}}^{(\mathrm{prim})}\rangle^2 - \frac{3P}{2\beta^2} - \frac{2}{\beta}\langle V_{\mathrm{TI}}\rangle\right] - \frac{m''(\lambda)}{m(\lambda)}\langle T_{\mathrm{TI}}^{(\mathrm{prim})}\rangle \tag{A.12}$$

In these expressions $T_{\mathrm{TI}}^{(\mathrm{prim})}$ is the fourth-order primitive kinetic energy estimator in eq 19.

■ ASSOCIATED CONTENT

Supporting Information

Three sections. The first is an investigation of the double well for a temperature of $T = 0.625$, for which the free energy as a function of λ is nonmonotonic. In the second section, we present the dependence of the free energy derivate on the number of path-integral beads and the value of λ for the protonated and deprotonated water dimer. Finally, the third section contains a detailed error analysis of all of the estimators using the block averaging technique. This material is available free of charge via the Internet at http://pubs.acs.org.

■ AUTHOR INFORMATION

Corresponding Author

*E-mail: mark.tuckerman@nyu.edu.

Notes

The authors declare no competing financial interest.

■ ACKNOWLEDGMENTS

This research was carried out on the High Performance Computing resources at New York University Abu Dhabi. O.M., Z.B., and M.E.T. acknowledge support from NSF CHE-1112292. R.D. and M.M. acknowledge support from the interdisciplinary program PEPS—Theoretical Physics and Its Interfaces—of French CNRS. The authors also acknowledge A. Pérez and O. A. von Lilienfeld for useful discussions concerning the derivation of presented in the Appendix.

■ REFERENCES

(1) Markland, T. E.; Berne, B. J. *Proc. Natl. Acad. Sci. U.S.A.* **2012**, *109*, 7988−91.
(2) Tomascak, P. B.; Widom, E.; Benton, D.; Goldstein, S. L.; Ryan, J. G. *Earth Planetary Sci. Lett.* **2002**, *196*, 227−238.
(3) Elliott, T.; Jeffcoate, A.; Bouman, C. *Earth Planetary Sci. Lett.* **2004**, *220*, 231−245.
(4) Vigier, N.; Decarreau, A.; Millot, R.; Carignan, J.; Petit, S.; France-Lanord, C. *Geochim. Cosmochim. Acta* **2008**, *72*, 780−792.
(5) Kirkwood, J. G. *J. Chem. Phys.* **1935**, *3*, 300.
(6) Zwanzig, R. W. *J. Chem. Phys.* **1954**, *22*, 1420.
(7) Zimmermann, T.; Vanicek, J. *J. Chem. Phys.* **2009**, *131*, 024111.
(8) Ceriotti, M.; Markland, T. E. *J. Chem. Phys.* **2013**, *138*, 014112.
(9) Hauser, A. W.; Schrier, J.; Schwerdtfeger, P. *J. Phys. Chem. C* **2012**, *116*, 10819−10827.
(10) Hankel, M.; Jiao, Y.; Du, A.; Gray, S. K.; Smith, S. C. *J. Phys. Chem. C* **2012**, *116*, 6672−6676.
(11) Jiao, Y.; Du, A.; Hankel, M.; Smith, S. C. *Phys. Chem. Chem. Phys.* **2013**, *15*, 4832−43.
(12) Pollock, E.; Ceperley, D. *Phys. Rev. B* **1984**, *30*, 2555−2568.
(13) Zhang, D. H.; Wu, Q.; Zhang, J. Z. H.; von Dirke, M.; Bačić, Z. *J. Chem. Phys.* **1995**, *102*, 2315.
(14) Tuckerman, M. E.; Marx, D.; Klein, M. L.; Parrinello, M. *Science* **1997**, *275*, 817−820.
(15) Pluhařová, E.; Mason, P. E.; Jungwirth, P. *J. Phys. Chem. A* **2013**, in press.

(16) Leung, K.; Rempe, S. B.; von Lilienfeld, O. A. *J. Chem. Phys.* **2009**, *130*, 204507.
(17) Herman, M. F.; Bruskin, E. J.; Berne, B. J. *J. Chem. Phys.* **1982**, *76*, 5150.
(18) Parrinello, M.; Rahman, A. *J. Chem. Phys.* **1984**, *80*, 860.
(19) Jang, S. J.; Jang, S. M.; Voth, G. A. *J. Chem. Phys.* **2001**, *115*, 7832−7842.
(20) Pérez, A.; Tuckerman, M. E. *J. Chem. Phys.* **2011**, *135*, 064104.
(21) Vuchowiecki, M.; Vanicek, J. *Chem. Phys. Lett.* **2013**, *588*, 11.
(22) Takahashi, M.; Imada, M. *J. Phys. Soc. Jpn.* **1984**, *53*, 3765−3769.
(23) Li, X.-P.; Broughton, J. Q. *J. Chem. Phys.* **1987**, *86*, 5094.
(24) Martyna, G. J.; Klein, M. L.; Tuckerman, M. E. *J. Chem. Phys.* **1992**, *97*, 2635.
(25) Tuckerman, M. E.; Berne, B. J.; Martyna, G. J.; Klein, M. L. *J. Chem. Phys.* **1993**, *99*, 2796.
(26) Martyna, G.; Tuckerman, M. E.; Tobias, D.; Klein, M. *Mol. Phys.* **1996**, *87*, 1117−1157.
(27) Tuckerman, M.; Berne, B. J.; Martyna, G. J. *J. Chem. Phys.* **1992**, *97*, 1990.
(28) Tuckerman, M. E.; Marx, D.; Klein, M. L.; Parrinello, M. *J. Chem. Phys.* **1996**, *104*, 5579.
(29) Yoshida, H. *Phys. Lett. A* **1990**, *150*, 262−268.
(30) Suzuki, M. *J. Math. Phys.* **1991**, *32*, 400.
(31) Mø ller, C.; Plesset, M. S. *Phys. Rev.* **1934**, *46*, 618−622.
(32) Frisch, M. J.; Trucks, G. W.; Schlegel, H. B.; Scuseria, G. E.; Robb, M. A.; Cheeseman, J. R.; Scalmani, G.; Barone, V.; Mennucci, B.; Petersson, G. A.; Nakatsuji, H.; Caricato, M.; Li, X.; Hratchian, H. P.; Izmaylov, A. F.; Bloino, J.; Zheng, G.; Sonnenberg, J. L.; Hada, M.; Ehara, M.; Toyota, K.; Fukuda, R.; Hasegawa, J.; Ishida, M.; Nakajima, T.; Honda, Y.; Kitao, O.; Nakai, H.; Vreven, T.; Montgomery, J. A.; Peralta, J. E.; Ogliaro, F.; Bearpark, M.; Heyd, J. J.; Brothers, E.; Kudin, K. N.; Staroverov, V. N.; Kobayashi, R.; Normand, J.; Raghavachari, K.; Rendell, A.; Burant, J. C.; Iyengar, S. S.; Tomasi, J.; Cossi, M.; Rega, N.; Millam, J. M.; Klene, M.; Knox, J. E.; Cross, J. B.; Bakken, V.; Adamo, C.; Jaramillo, J.; Gomperts, R.; Stratmann, R. E.; Yazyev, O.; Austin, A. J.; Cammi, R.; Pomelli, C.; Ochterski, J. W.; Martin, R. L.; Morokuma, K.; Zakrzewski, V. G.; Voth, G. A.; Salvador, P.; Dannenberg, J. J.; Dapprich, S.; Daniels, A. D.; Farkas, Ö.; Foresman, J. B.; Ortiz, J. V.; Cioslowski, J.; Fox, D. J. *Gaussian 09*, Revision C.01; Gaussian, Inc., Wallingford, CT, 2009.
(33) Bahn, S.; Jacobsen, K. *Comput. Sci. Eng.* **2002**, *4*, 56−66.
(34) Cao, J.; Berne, B. J. *J. Chem. Phys.* **1989**, *91*, 6359.
(35) Pérez, A.; von Lilienfeld, O. A. *J. Chem. Theory Comput.* **2011**, *7*, 2358−2369.
(36) Suzuki, K.; Tachikawa, M.; Shiga, M. *J. Chem. Phys.* **2013**, *138*, 184307.
(37) Yamamoto, T. M. *J. Chem. Phys.* **2005**, *123*, 104101.
(38) Glaesemann, K. R.; Fried, L. E. *J. Chem. Phys.* **2002**, *117*, 3020.
(39) Marx, D.; Parrinello, M. *J. Chem. Phys.* **1996**, *104*, 4017.
(40) Tuckerman, M. E.; Marx, D.; Klein, M. L.; Parrinello, M. *J. Chem. Phys.* **1996**, *104*, 5579.
(41) Ceriotti, M.; Brain, G. A. R.; Riordan, O.; Manolopoulos, D. E. *Proc. Royal Soc. A - Math., Phys., Eng. Sci.* **2012**, *468*, 2.